

VALIDATION OF ASAR WAVE MODE LEVEL 2 PRODUCT

H. Johnsen¹, G. Engen¹, B. Chapron², N. Walker³, J. Closa⁴

¹NORUT IT, N-9291 Tromsø, Norway, Tel: +47 77629400, Fax: (+01), Email: harald.johnsen@itek.norut.no

²Dpt. DRO/Océanographie Spatiale, IFREMER, BP 70 29280 Plouzane France, Email: bchapron@ifremer.fr

³SERCO spa for ESA/ESRIN, Email: nicholas.walker@esa.int

⁴Altamira spa for ESA/ESRIN, Email: josep.closa@esa.int

ABSTRACT

A geophysical validation of the ASAR Wave Mode Level 2 product is performed using ASAR Wave Mode data acquired in the period May 2002 – October 2002. The ASAR Wave Mode data have been co-located with ECMWF WAM spectra and wind speed data, and also some with NOAA buoy data. The paper presents calibration results and a comparison of wind speed and wave spectral parameters from the co-located data sets. The geophysical derived calibration constants using either ECMWF wind field or NOAA buoy wind field agree to within 0.5dB with the engineering calibration constant using transponder or the rain forest measurements. The geophysical validation of wind and wave parameters shows very good agreement in terms of mean wave periods, T_p, T_p^{12} , but the ASAR tends to measure a longer mean swell period than predicted by WAM. We also see that the ASAR Level2 swell spectra are on average narrower than the WAM swell spectra. For the significant waveheight, H_s , we see saturation effects at high sea-states. Less saturation effects observed when considering only H_s^{12} . Good correlation is also observed for the mean spectral wave direction, Φ . The saturation in H_s is mostly due to the well-known effect of azimuth roll-off, which increases with increasing wind sea states.

The performance of the Level 2 product in terms of RMS and bias are established and tabulated for various wave spectral parameters. It is also observed that the performance improves in areas of high swell index.

1 INTRODUCTION

ASAR Wave Mode Level 2 products [1] provide estimates of the SAR ocean wave spectra and the local wind speed. We have performed a geophysical calibration of the Wave Mode radar cross section and a validation of ocean wave spectral parameters and wind speed of the Level 2 product using co-located ECMWF WAM and NOAA buoy data. A total of 21 sequences of orbits were used, covering different ocean regions. Best performance is observed in the open ocean where the energy of swell system dominates the wave spectra (i.e. high swell index areas). A similar analysis was done in [3], considering only to high swell index areas of central Ocean Pacific. This work extends the previous work by including data from other areas as well.

2 VALIDATION RESULTS

2.1 Geophysical Calibration

The wind speed retrieval algorithm implemented in the Level 2 product is based on combining the ASAR cross section with the CMOD-Ifremer backscatter model. It therefore requires the input SAR SLC data to be absolutely calibrated. This can be done in two ways, either by using the “engineering calibration constant” derived by transponder measurements or by performing a geophysical calibration against the model itself, using co-located “ground truth” data. We have compared these two approaches with good agreement, even with this relatively small data set. We achieve for the geophysical calibration constant a value of 47.19dB using the NOAA buoys as the in-situ truth (Fig.1), and a value of 47.75 using the ECMWF wind field as the in-situ truth (Fig. 1). The transponder and rain forest calibration constant was measured to 47.38dB.

We have also investigated the relationship between the kinematics and the roughness parameters of the Level 2 product, and shown how it can be used to monitor the absolute gain of the system (Fig.2)[2].

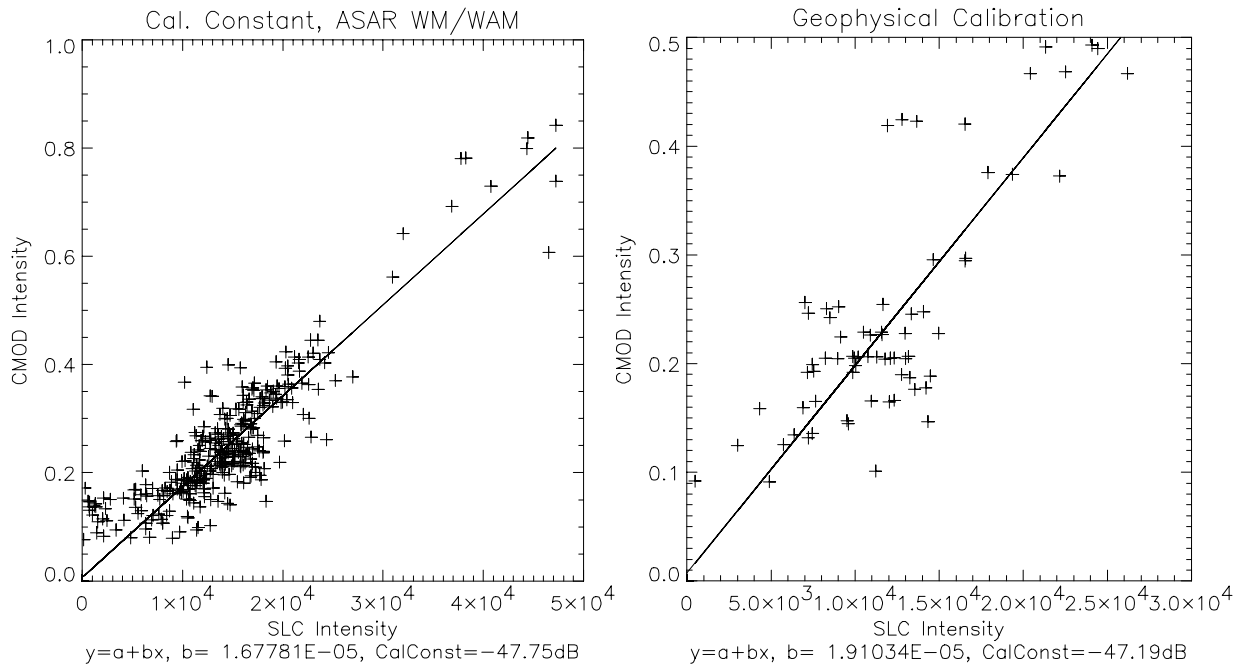


Fig. 1. CMOD-Ifremer predicted intensity (using collocated in-situ wind speed and direction) versus SLC detected intensity for the ASAR Wave Mode Level 1b product. Left: Using ECMWF wind field, Right: Using NOAA Buoy wind field.

We have also validated the kinematic parameter (non-linear cut-off) versus the roughness parameter (radar cross section) of the Level 2 product (Fig.2 (left)), and shown how it can be used to monitor the gain of the system (Fig.2 (right)).

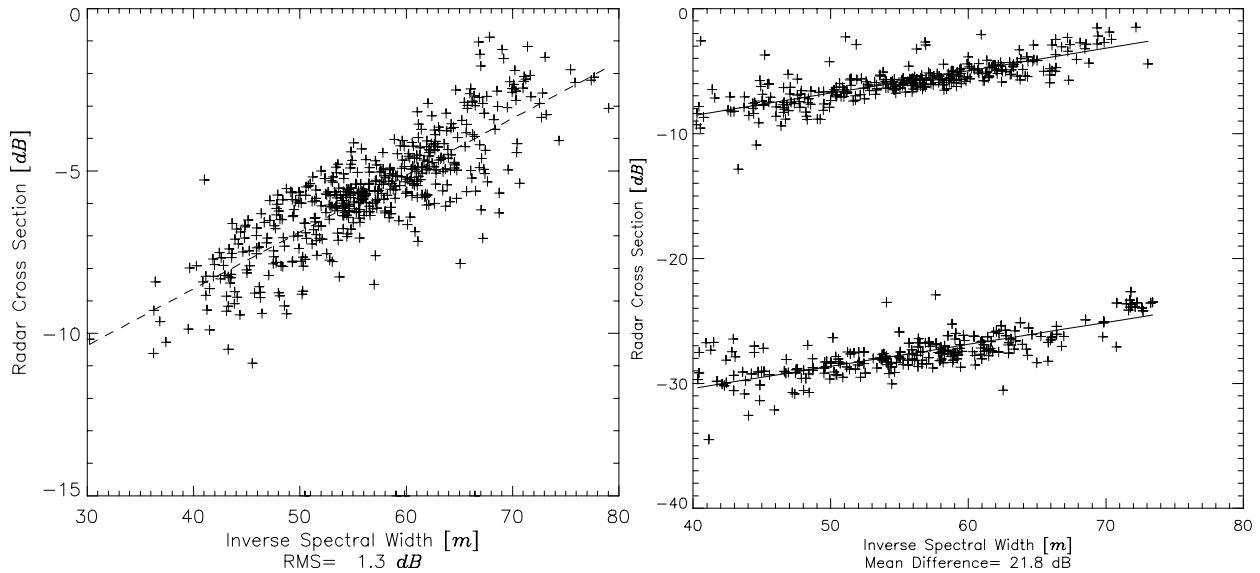


Fig. 2. Left: Normalized radar cross section versus asymptotic inverse azimuth spectral width for Envisat ASAR Wave Mode Level 2 product. Right: Same parameters plotted before and after the change of processor gain.

Fig.2 , left plot, shows a linear relationship between the kinematic and the roughness parameter with an RMS of 1.3dB. This property has been used in right plot to estimate the change in processor gain that was introduced in the processor in July 2002. The change in gain is from Fig.2 (right plot) estimated to 21.8dB which is similar to the value imposed to the processor. We conclude that using the roughness/kinematic properties we can monitor the drift in gain to within 1dB. This agrees well with the achievements published by Engen and Johnsen (1998) using ERS Image Mode data.

2.2 SAR Wave Spectra Validation

The geophysical validation was achieved by comparing wave spectral parameters extracted from the wave spectra measured by the ASAR Level 2, or as predicted by the ECMWF WAM model. The ASAR Wave Mode Level 2 spectra are displayed on a log-polar grid in the wavenumber and direction domain, $F(k, \varphi)$. The frequency-, $F(f)$, directional-, $\psi(\varphi)$, and mean directional spectra, $\phi(f)$ are then derived from the Level 2 and WAM wave spectra, $F(k, \varphi)$ according to the formulas:

$$(1) \quad F(f) = \int F(k, \varphi) k \cdot dk d\varphi \cdot d\varphi$$

$$(2) \quad \psi(\varphi) = \int F(k, \varphi) dk$$

$$(3) \quad \phi(f) = \tan^{-1} \left(\frac{\int F(k, \varphi) \sin \varphi d\varphi}{\int F(k, \varphi) \cos \varphi d\varphi} \right)$$

where $dkdf = 4\pi\sqrt{k/g}$. The significant wave-heights, H_s, H_s^{12} mean periods, T_p, T_p^{12} , and mean wave direction, Φ are then computed as:

$$(4) \quad H_s = 4 \sqrt{\int_{f_{\min}}^{f_{\max}} F(f) df}, \quad H_s^{12} = 4 \sqrt{\int_{f_{\min}}^{1/12} F(f) df}$$

$$(5) \quad T_p = \frac{\int_{f_{\min}}^{f_{\max}} F(f) f^{-1} df}{\int_{f_{\min}}^{f_{\max}} F(f) df}, \quad T_p^{12} = \frac{\int_{f_{\min}}^{1/12} F(f) f^{-1} df}{\int_{f_{\min}}^{1/12} F(f) df}$$

$$(6) \quad \Phi = \tan^{-1} \left(\frac{\int_{f_{\min}}^{f_{\max}} F(f) \sin(\phi(f)) df}{\int_{f_{\min}}^{f_{\max}} F(f) \cos(\phi(f)) df} \right)$$

where f_{\min}, f_{\max} are the lowest and highest frequencies in the spectrum to be computed over. Similar parameters can be derived from the ECMWF WAM spectra. The azimuth cut-off is an important parameter for SAR Ocean imaging, and it can be related to the underlying wave spectrum through the formula:

$$(7) \quad \lambda_{orb} = \left(\frac{R}{V} \right)^2 \int_0^{2\pi} \int_0^{\infty} df d\varphi f^2 \tilde{F}(f, \varphi)$$

where now \tilde{F} is the total underlying ocean wave spectrum (all scale lengths). We see that the cut-off given by λ_{orb} is more sensitive to the wind sea spectrum than to the swell, thus more dependent on the local wind speed than on the significant wave-height.

In Fig. 3 we show examples of $F(f)$ and $\psi(\varphi)$ spectra computed from co-located ASAR and ECMWF WAM data.

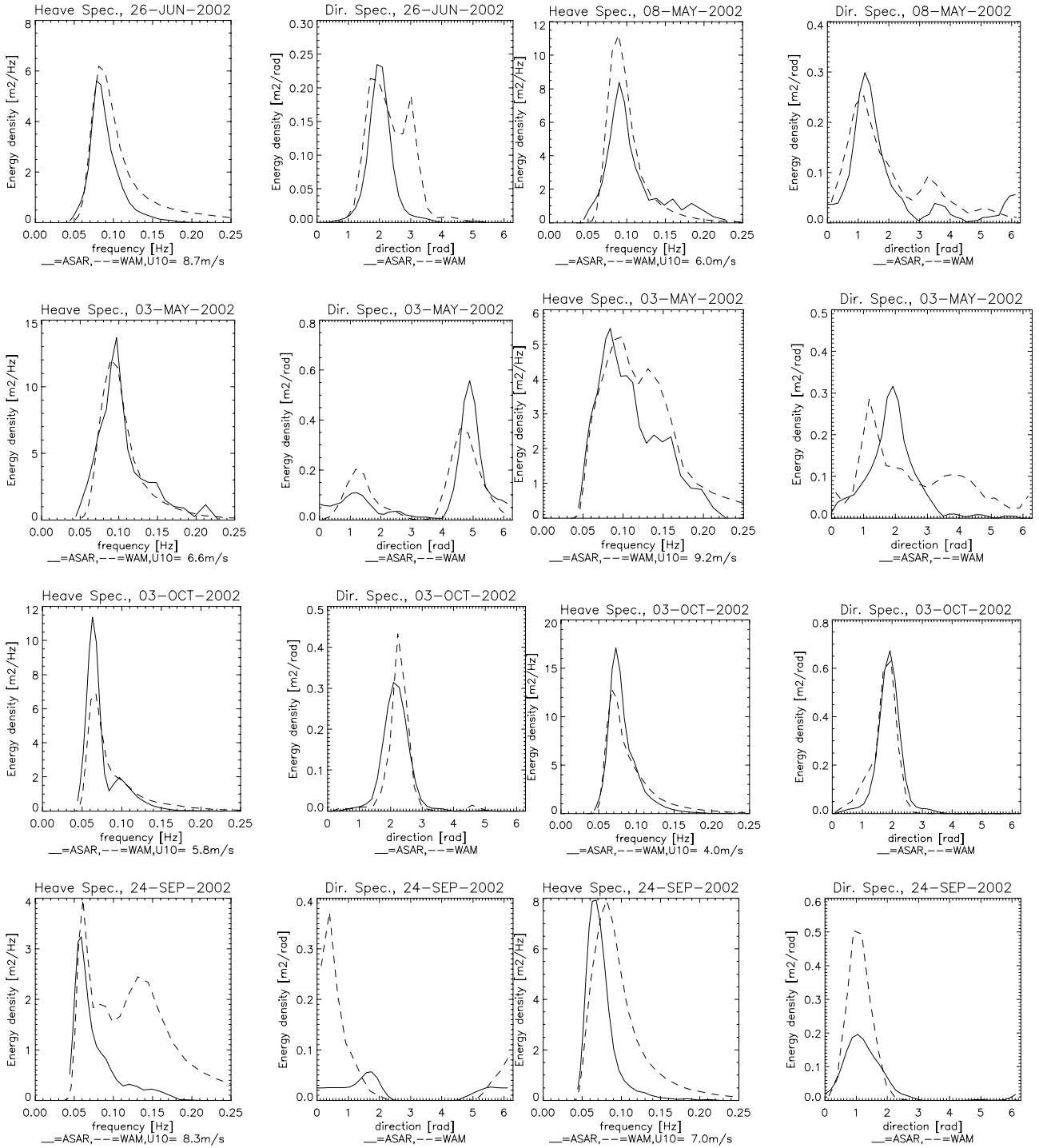


Fig. 3. Examples of one-dimensional frequency and directional spectra extracted from ASAR Level 2 wave spectra (full line), WAM wave spectra (dotted line).

We see from Fig.3 that the ASAR Level 2 product predicts swell values comparable with the WAM, but only rarely for the wind sea spectrum, which as was discussed earlier, is expected. However, we note that the ASAR Level 2 swell spectra are narrower and that they tend to peak at lower frequencies. This is quantified more precisely in the following. Further statistics derived from the spectral parameters are shown in the plots, Fig. 4 – Fig. 9. A one-to-one linear model is assumed for describing the relationships between the ASAR and the WAM derived parameters. The RMS value describes the standard deviation error with respect to the model. First the wind speed comparison is shown and then the wave spectral parameters. Fig. 4 shows the comparison between ASAR Wave Mode Level 2 and ECMWF wind speed for different data sets.

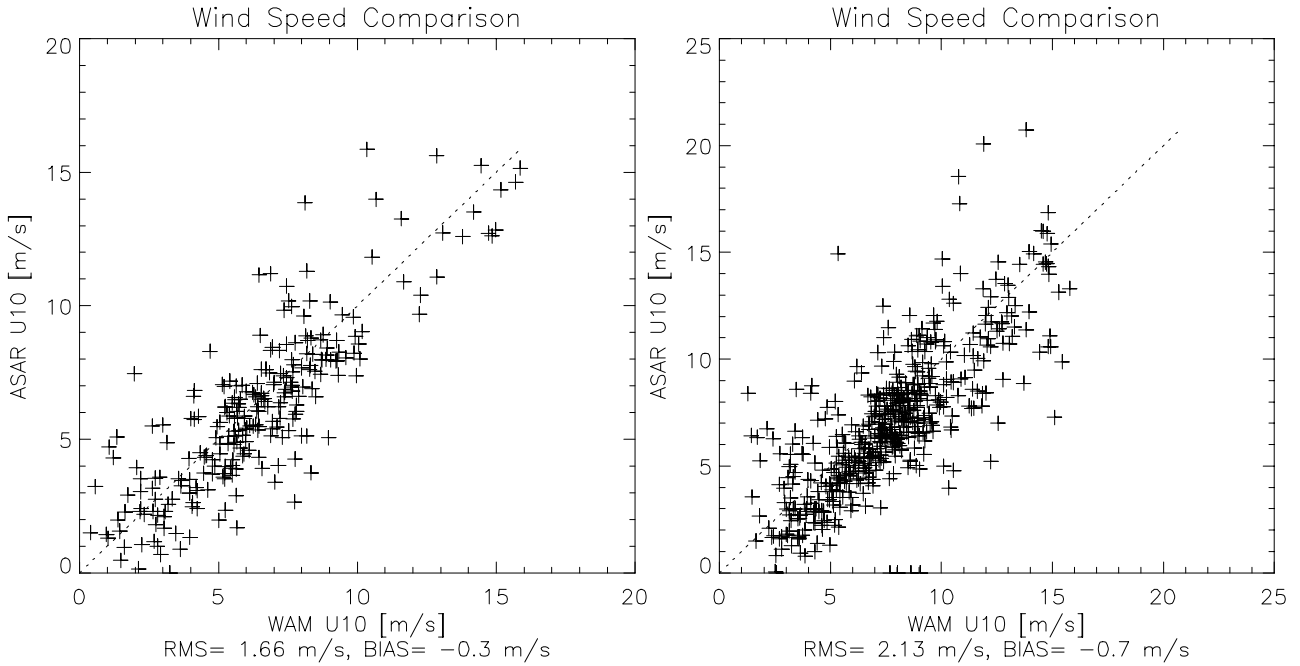


Fig. 4. ASAR Level 2 wind speed versus co-located wind speed from the ECMWF atmospheric model. The ECMWF wind direction is used in the Level 2 processing. The two plots represent different periods of the year and different areas.

Fig. 4 shows that the ASAR Level 2 product provides estimates of wind speed with an RMS error of around 2 m/s with respect to the ECMWF wind speed.

In Fig. 5 and Fig. 6 we compare the ASAR Level 2 significant wave-heights, H_s, H_s^{12} and mean wave periods, T_p, T_p^{12} against corresponding parameters from WAM spectra. The wave parameters are computed for both the total spectrum and for the waves with period above 12 sec. The latter is assumed to cover wavelengths that on average can be resolved by the ASAR system.

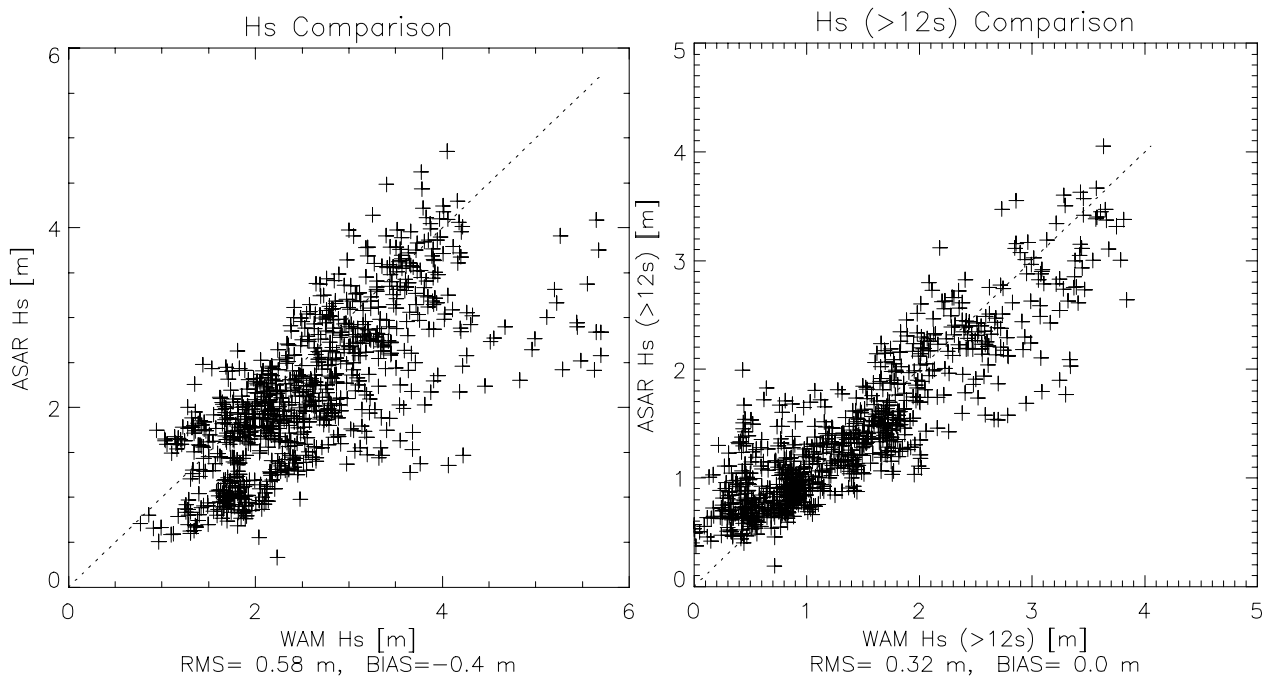


Fig. 5. ASAR Wave Mode Level 2 significant waveheight versus ECMWF WAM waveheight computed over the entire spectrum (left), and only for waves with period longer than 12 sec (right).

Fig. 5 shows that the WAM and ASAR H_s correspond well for low sea states ($H_s < 3\text{m}$), but that the ASAR H_s saturates for higher sea states. If only waves with periods longer than 12 sec are used, we see that the saturation becomes less pronounced with an RMS error of 0.32m. The saturation effect is most likely to be caused by the azimuth cut-off effect, which increases with increasing sea state. This is shown more clearly by plotting the difference in H_s as function of wind speed, as shown in Figure 5.

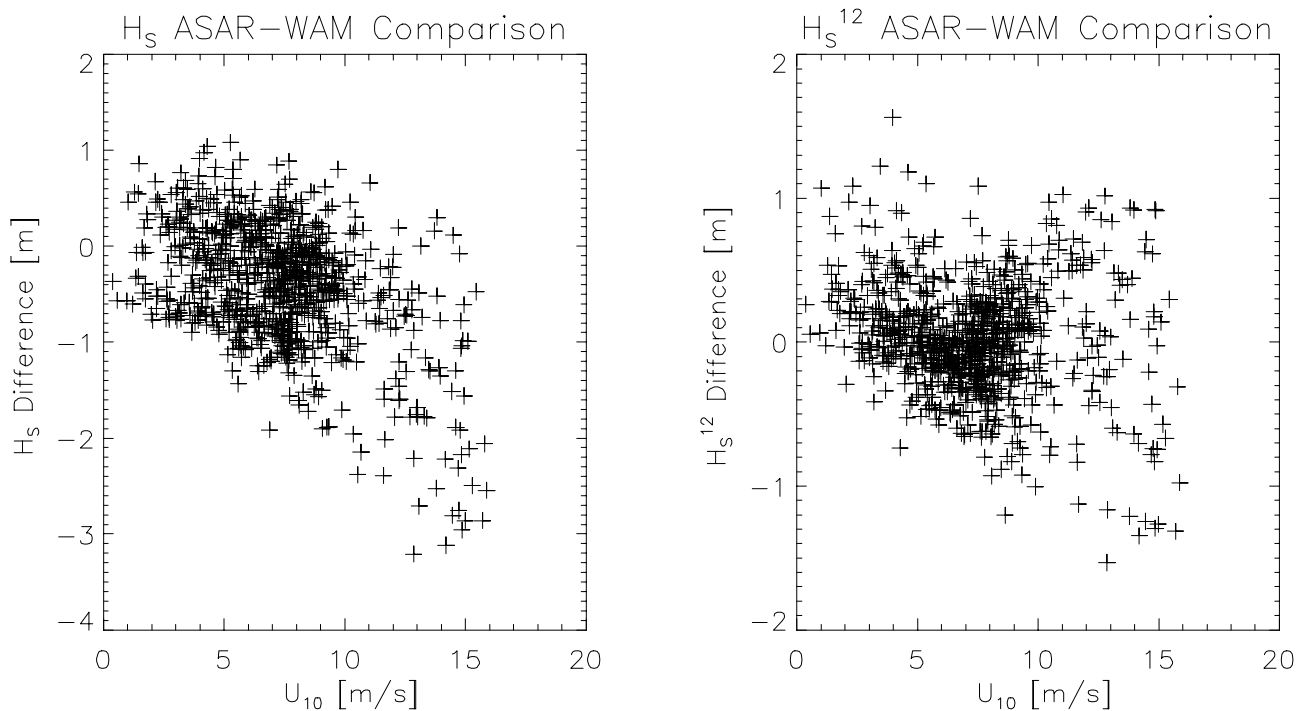


Fig. 6. Difference between ASAR Level 2 and WAM H_s, H_s^{12} as function of U_{10} from ECMWF atmospheric model.

Fig. 6 shows that the deviations in H_s increase with increasing wind speed, and that if we consider only H_s^{12} the effect is less pronounced. The observed trends can be explained by the fact that the azimuth cut-off is strongly dependent on the wind sea spectrum, as also predicted by the equation for λ_{orb} .

In Fig. 7 we show the comparison of the co-located ASAR and WAM for the mean wave periods, T_p and T_p^{12} .

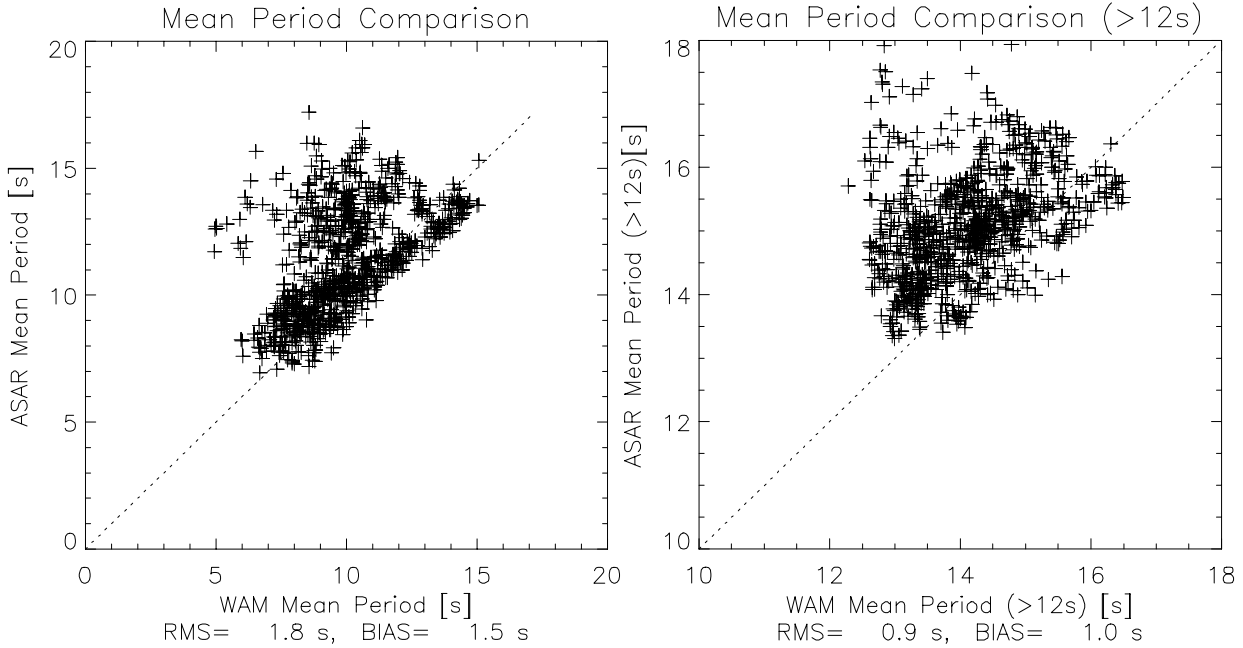


Fig. 7. ASAR Wave Mode Level 2 mean wave period versus collocated ECMWF WAM mean period computed over the entire spectrum (left), and only for waves with period longer than 12 sec (right).

Fig. 7 show that the WAM mean periods and the ASAR Level 2 mean wave periods are well correlated. The overall good agreement can be explained by the way the T_p favours lower frequency waves (see Eq. 6 for T_p). The plots in Fig.7 show that the SAR measures a slightly larger mean wave period than the WAM, which can partly be explained again by the azimuth smearing effect. If we restrict the computation to waves with period larger than 12 sec, both the bias and the RMS error are reduced (see Table 1, Fig.7 left plot). However, we still have a significant bias (1.0s) for the mean period of the swell part of the spectrum. The left plot of Fig.7 also shows almost two distinct clouds of data. The one aligned along the dotted line is mainly the central and east pacific, while the rest is scattered from different areas around the world. This shows that the Level 2 performs best in swell dominated areas, which is also as expected. The histograms of mean period difference between Level 2 and WAM corresponding to Fig.7 are shown in Fig.8.

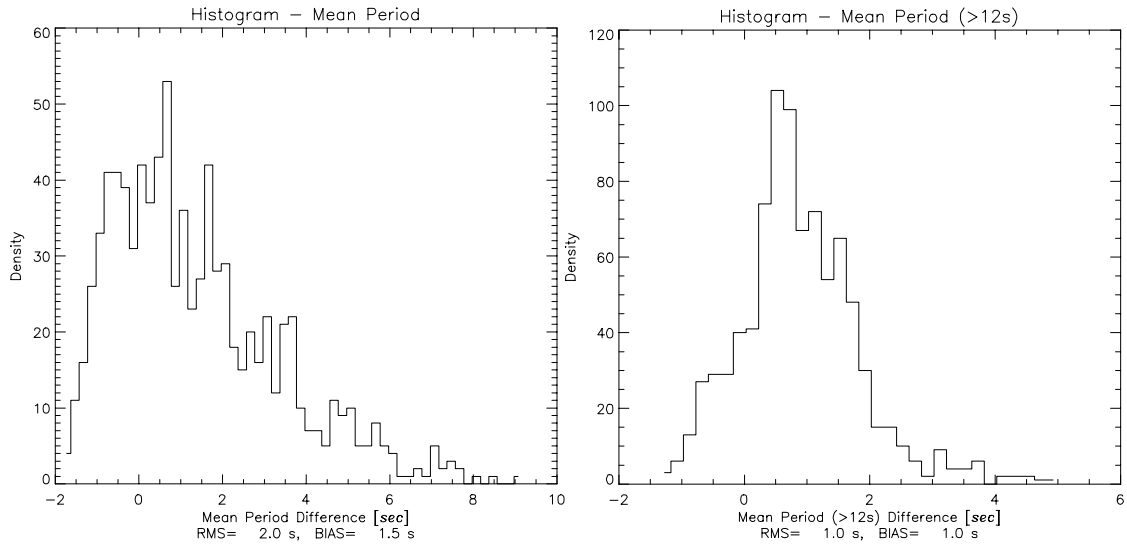


Fig. 8. Histogram of difference in ASAR Wave Mode Level 2 and ECMWF WAM mean wave period for waves with periods longer than 12s (right) and for all wave periods (left).

Fig.8 shows a skewed histogram considering the whole spectrum (left), while restricting the computation to waves longer than 12 sec a Gaussian shaped histogram is observed (right). However, a bias of around 1.0 s is observed even considering only the swell part of the spectra. These observations indicate that the bias of 1.0 s observed in Fig.8 is not not caused by cut-off effects.

In Fig. 9 we compare the difference of the ASAR Level 2 and WAM mean wave direction. The mean wave direction is computed according to the formula for Φ (see Eq. 7) for all periods, and for only waves with periods larger than 12 sec.

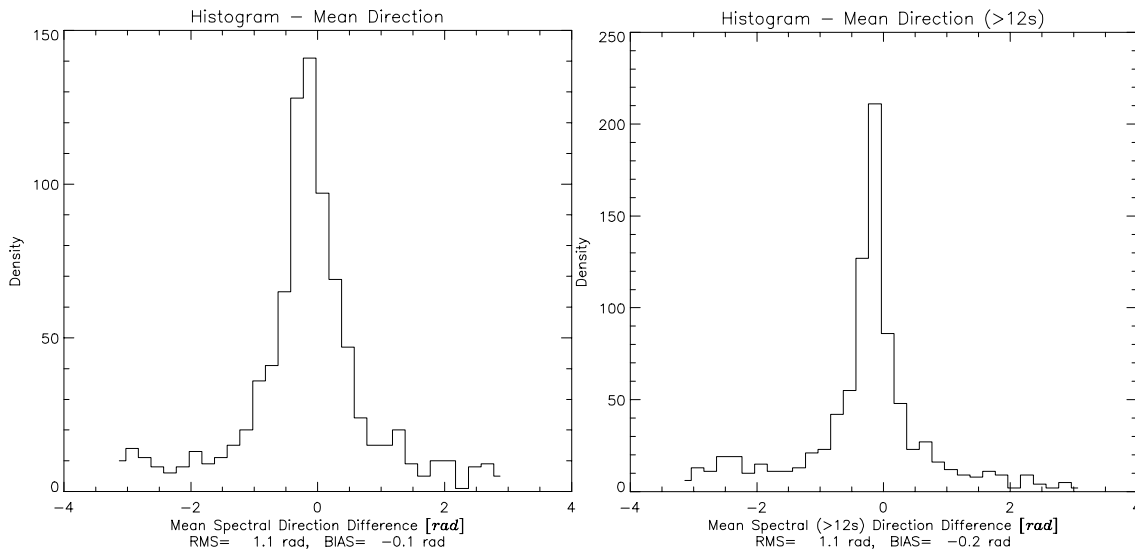


Fig. 9. Histogram of difference in ASAR Wave Mode Level 2 and ECMWF WAM mean wave direction for waves with periods longer than 12s (right) and for all wave periods (left).

Fig.9 shows Gaussian shaped histograms with a dominant peak around zero and a width corresponding to the RMS values. We see that the width of the central peak of the histogram decreases when only considering waves with periods longer than 12 sec. This is expected because of the cut-off affecting the direction of the shorter wavelengths of the SAR spectrum.

In Table 1 we have summarised the results of the calibration and validation of the ASAR Wave Mode Level 2 wave spectra using co-located ECMWF WAM spectra.

Table 1: RMS errors of a one-to-one linear model between in-situ and ASAR Level 2 U_{10} , H_s , T_p , Φ . The in-situ values are taken from the ECMWF WAM model. Geophysical versus engineering calibration constant are also given (T =Transponder, R =Rain forest, B =NOAA buoys, M =ECMWF model)

H_s^{12} (m)		H_s (m)		T_p^{12} (s)		T_p (s)		U_{10} (m/s)		Φ (rad)		Cal.Const	
RMS	Bias	RMS	Bias	RMS	Bias	RMS	Bias	RMS	Bias	RMS	Bias	Eng. T/R	Geo. B/M
0.5	-0.4	0.3	0.0	1.8	1.5	0.9	1.0	2.1	-0.7	1.1	-0.2	47.38	47.19
												47.38	47.75

3 CONCLUSIONS

Validation of the ASAR Wave Mode Level 2 products processed from ASAR Wave Mode shows that the algorithms perform well in terms of providing a two-dimensional, ambiguity free wave spectrum within the SAR imaging domain for most of cases imaged. The estimate of the wind speed and the mean wave period correlates well with the co-located ECMWF wind speed. However, a bias of 1.0s is observed for the mean swell period showing that the ASAR tends to measure a longer swell mean period than predicted by WAM. We also observe that the ASAR swell frequency spectrum is narrower than the co-located WAM swell spectrum. Strong correlations are also observed for the mean and peak propagation direction although the RMS is around 1 radian considering the whole data set. The significant waveheight correlates also well, especially for the swell part of the spectrum. Estimate of the ASAR derived significant wave-height saturates at high wind speeds (>10m/s). This can be caused by a combination of the azimuth cut-off effect, and an underestimation of the orbital velocity variance (i.e. the quasi-linear cut-off). At high wind speeds, where the saturation effect dominates, the non-linear contribution starts to be dominant in the spectrum. The estimation of the orbital velocity variance from the spectrum becomes coloured by the non-linear contribution, causing the quasi-linear cut-off to be underestimated. This in turn causes H_s of the quasi-linearly inverted spectra to become less than expected. Improper modelling of the transfer function can also be a cause for the observed saturation effect. Further studies will be undertaken when more data becomes available.

Acknowledgement:

The work was co-funded by the Research DG of the European Commission under contract EVG1-CT-2001-00051, "EnviWave", and by ESA/ESTEC under contract No. 12909/98/NL/PR, "Envisat ASAR Wind&Wave Measurements from Wave Mode Level 1b product".

4 REFERENCES

- [1] Engen G., Johnsen H., Høgda K.A., Chapron B., "Envisat ASAR Level 2 Wave Mode Product Algorithm Specification – Software Requirement Document", NORUT IT Doc. No.: 650/1-01,v2.2.5, Oct., 2001.
- [2] G. Engen, H. Johnsen, "A new method for calibration of SAR images", Proceedings of CEOS SAR Workshop, October 26-29, Toulouse, 1999.
- [3] Johnsen H., Engen G., Chapron B., Walker N., Closa J., "Validation of ASAR Wave Mode Level2 Product", Proc. of Envisat Cal/Val Review, ESA SP-520, 9-13 September 2002.